REPORT DOCUMENTATION PAGE

Form Approved
OMB No. 0704-0188

1. REPORT DATE *(DD-MM-YYYY)*	2. REPORT TYPE	3. DATES COVERED *(From - To)*
	Technical Paper	

4. TITLE AND SUBTITLE

Please see attached

5a. CONTRACT NUMBER

5b. GRANT NUMBER

5c. PROGRAM ELEMENT NUMBER

6. AUTHOR(S)

5d. PROJECT NUMBER
2308

5e. TASK NUMBER
M13C

5f. WORK UNIT NUMBER
346057

7. PERFORMING ORGANIZATION NAME(S) AND ADDRESS(ES)

ERC

8. PERFORMING ORGANIZATION REPORT

9. SPONSORING / MONITORING AGENCY NAME(S) AND ADDRESS(ES)

Air Force Research Laboratory (AFMC)
AFRL/PRS
5 Pollux Drive
Edwards AFB CA 93524-7048

10. SPONSOR/MONITOR'S ACRONYM(S)

11. SPONSOR/MONITOR'S NUMBER(S)
Please see attached

12. DISTRIBUTION / AVAILABILITY STATEMENT

Approved for public release; distribution unlimited.

13. SUPPLEMENTARY NOTES

14. ABSTRACT

15. SUBJECT TERMS

16. SECURITY CLASSIFICATION OF:			17. LIMITATION OF ABSTRACT	18. NUMBER OF PAGES	19a. NAME OF RESPONSIBLE PERSON
a. REPORT	b. ABSTRACT	c. THIS PAGE			Leilani Richardson
Unclassified	Unclassified	Unclassified	A		19b. TELEPHONE NUMBER *(include area code)* (661) 275-5015

FILE

MEMORANDUM FOR PRS (In-House/Contractor Publication)

FROM: PROI (STINFO) 06 Mar 2001

SUBJECT: Authorization for Release of Technical Information, Control Number: **AFRL-PR-ED-TP-2001-045**
Chehroudi, B.; Cohn, R.; Talley, D., "The Behavior of Cryogenic Shear Layers under Supercritical Conditions"

2nd International Symposium on Turbulence and Shear Flow Phenomena (Statement A)
(Stockholm, Sweden, 27 June 2001) (Deadline: 15 Mar 2001)

THE BEHAVIOR OF CRYOGENIC SHEAR LAYERS UNDER SUPERCRITICAL CONDITIONS

B. Chehroudi
Engineering Research Consultants, Inc.
10 E. Saturn Blvd., Edwards AFB, CA, USA 93524-7680
Bruce.Chehroudi@edwards.af.mil

R. Cohn and D. Talley
Air Force Research Laboratory, Space and Missile Propulsion Division
AFRL/PRSA, 10 E. Saturn Blvd, Edwards AFB, CA 93524-7680
Richard.Cohn@edwards.af.mil
Douglas.Talley@edwards.af.mil

Abstract

Recent experience gained at AFRL with the injection of cryogenic fluids into high back-pressures is summarized. In the experimental investigations described, a jet of a cryogenic fluid, typically liquid N_2, is injected into a chamber whose ambient pressure is varied to values exceeding the critical pressure of the injectant. The structure of the jet and the shear layer between the jet and the ambient has been examined. Results from visualization, jet growth rate, fractal analysis, and Raman scattering measurements indicate that the behavior of the injected fluid changes from spray-like behavior to gas jet-like behavior as pressure increased.

Introduction

In recent years, combustion chamber pressures have increased in order to realize performance and/or efficiency benefits in a wide range of propulsion and energy conversion applications. In some cases, this has resulted in the injected propellant(s) experiencing ambient pressures exceeding their critical pressure(s). For example, in the cryogenic liquid hydrogen/liquid oxygen Space Shuttle Main Engine, the thrust chamber pressure is about *22.3 MPa*. Thrust chamber pressures for the Vulcain (Ariane 5) engine have been recorded to reach up to *10 MPa*. Both of these pressures exceed the critical pressure of P_{cr} = *5.043 MPa* for liquid oxygen. In these applications, the initial temperature of the oxygen is below its critical temperature (T_{cr} = *154.58 K*), and then undergoes a transition to a supercritical temperature as the oxygen is mixed and burned in the combustion chamber.

For single component fluids, the distinct difference between the gas and liquid phases disappears when either the pressure exceeds the critical pressure or the temperature exceeds the critical temperature. Near the critical point, Surface tension and the enthalpy of vaporization vanish, and large variations in the density, thermal conductivity, and mass diffusivity occur. For multi-component fluids, the solubility of the gas phase in the liquid phase increases as pressure approaches the critical pressure, and mixture effects need to be taken into account in calculating the critical properties. The critical properties of mixtures are referred to as the "critical mixing temperature" and the "critical mixing pressure" (Bruno and Ely, 1991). The critical mixing pressure can be many times the critical pressure of the compounds of interest as seen in Woodward and Talley (1996).

Previous efforts, for example, Newman and Brzustowski (1971), Mayer, *et al.* (1996), and Woodward and Talley (1996) have reported a gas jet-like visual appearance at a supercritical chamber temperature and pressure with no evidence of droplets. Anderson et al., Decker et al., Oschwald and Schik (1999), Oschwald et al. (1999), and Chehroudi *et al.* (2000) have used Raman scattering to investigate the structure of a cryogenic nitrogen jet under supercritical conditions. Decker *et al.* (1998) observed a smooth transition from the high-density core of a cryogenic, N_2 jet to the more rarefied, warmer N_2 in the ambient outer region. There was no distinct phase interface. The density radial profile was never observed to have a top hat profile, even as close as 2.5 diameters. Based on limited tests, they concluded that the thermodynamic state of an injected supercritical fluid was of prime importance in determining the jet growth, and not the injection velocity or momentum.

The objective of this paper is to concisely present the experimental and modeling experience gained thus far at AFRL on injecting cryogenic fluids at subcritical to supercritical pressures. The structural features of the jet and the shear layer between the jet and the ambient will be described. An initial attempt has been made to model the measured growth rate of the jet shear layer.

Experimental Apparatus

The experimental apparatus has been thoroughly described in Woodward and Talley (1996) and

Chehroudi, *et al.* (1999). The apparatus is capable of injecting cryogenic fluids into ambient pressures as high as *137* atm. For the results reported, a cryogenic jet is injected through a sharp-edged stainless steel tube with a length l = *50 mm* and having inner and outer diameters measuring d_e = *0.254 mm* and d_o = *1.59 mm* respectively. The Reynolds numbers in these studies ranged from *25,000* to *70,000*. This results in l/d_e = *200*, which is sufficient to ensure fully developed turbulent pipe flow at the exit plane. The rig is fully instrumented to measure pressure, temperature, and mass flow rate of the injected fluid.

Images of the evolving shear layer have been acquired by both shadowgraph and spontaneous Raman scattering. In the interest of space, we will concentrate the majority of this paper on the shadowgraph results.

Visual Appearance Changes in Cryogenic Jets and Shear Layers

Figure 1 (top row) shows representative images of a jet of liquid nitrogen (LN_2) (P_{cr} = *3.39 MPa*, T_{cr} = *126.2 K*) injected at an initial temperature of *99-110 K* into room temperature *(300 K)* gaseous nitrogen (GN_2). For the results presented here, the chamber pressure was normalized by the critical pressure of the pure fluid in the jet; $P_r = P_{chamber}/P_{cr}$. The bottom row of Figure 1 shows the jet shear layer. Generally, it is apparent that as pressure is increased, the jet width increases and the structure of the shear region changes from being dominated by droplets to being dominated by finger-like regions. The results presented here are not unique to the injection of liquid nitrogen. Similar results have been found injecting liquid oxygen into gaseous nitrogen.

In column (a), where the chamber pressure was subcritical, the jet had a classic liquid-like appearance. Surface instabilities grew downstream from the injector and very fine drops were ejected from the jet. At this pressure, the Ohnesorge number was approximately $2.8x10^{-3}$. This corresponds to a second wind-induced atomization regime in Reitz and Baracco (1979).

Major structural and interfacial changes occurred at P_r = *1.03*. Above this P_r, drops were no longer detected and regular finger-like entities were observed at the interface. Rather than breaking up into droplets, the interface dissolved at different distances from the dense core. These structures are illustrated at a P_r =*1.22* in column (b) of Fig. 1. This change in the morphology of the mixing layer is evidently due to the reduction in the surface tension as the critical pressure is exceeded. The enthalpy of vaporization also vanishes because of this transition.

As chamber pressure was further increased, the length and thickness of the dense core decreased, and the jet began to appear similar to a turbulent gaseous jet injected into a gaseous environment.

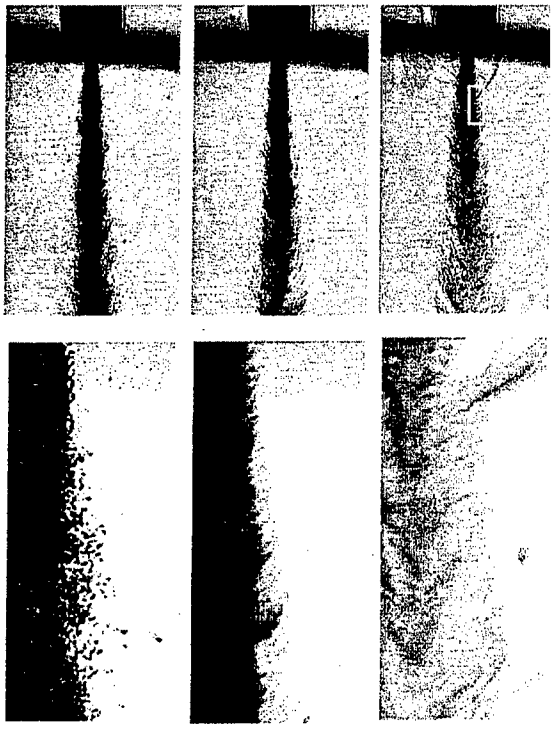

(a)	(b)	(c)
Pr=0.91	Pr=1.22	Pr=2.71
Re=75,281	Re=66,609	Re=42,830

Figure 1. LN_2 injected into room temperature nitrogen at different pressures. The bottom row contains magnified images of the top row in order to examine the shear layer.

This is illustrated in column (c). Any further droplet production, and consequently any additional atomization regimes, were completely surpressed.

Jet and Shear Layer Growth Rates

In order to compare with classical Cartesian mixing layer theory, the initial growth rate of the jets was measured at l/d_e < *28* from the jet exit. As discussed by Chehroudi *et al.* (1999), this distance was well within the mixing layer region. The results were then plotted in Figure 2 as the tangent of the spreading angle *vs.* the chamber-to-injectant density ratio. Overlaid on top of the present data are the results of other researchers. Because the present results span both gas-like and liquid-like behavior, it was necessary to plot the growth rates of both sprays and turbulent jets. This results in a plot that is unique in that it spans nearly four orders of magnitude in density ratio and compares growth rates for both sprays and turbulent jets.

We will first examine the subcritical region of Figure 2. A more complete description can be found in Chehroudi *et al.* (1999). In this region, the LN_2 jet appears visually to have spray-like characteristics, as seen in Figure 1a. The growth rate of this jet approaches that seen in spray measurements such as Reitz and Bracco (1979), plotted in Figure 2. The curves in these plots

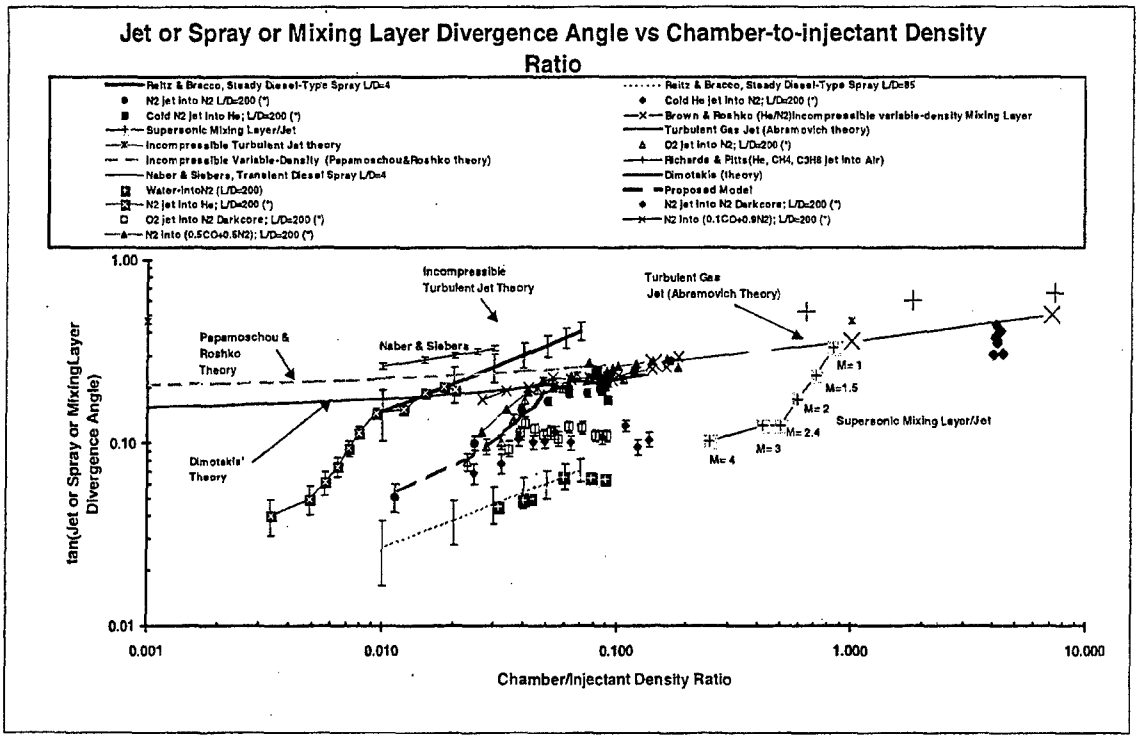

Figure 2. Tangent of the visual spreading angle versus the chamber-to-injectant density ratio. Data shown with an asterisk (*) were taken at AFRL.

represent the predictions of atomization theory, while the error bars represent the extent of experimental scatter around the theoretical predictions. Reitz and Bracco's data show the well-known result that the initial spreading rates of sprays from plain round orifices are sensitive to the internal L/d_e. However, in comparing the shape of the curves, their data for $L/d_e = 85$ closely corresponds to the LN_2 jet data at $L/d_e = 200$. In both of these cases, the flow is fully developed. In data not plotted in Fig. 2, the spreading rate for the LN_2 data effectively merges with the Reitz and Bracco (1979) curve at low density ratios.

As the density ratio is increased into the transition region (as seen in Figure 1b), the jet and shear layer growth rate also increases. Near the critical pressure, the rate of increase becomes much steeper. Note that the abrupt change occurs at different density ratios for the different data sets in Figure 2 because the data sets correspond to different mixtures with different critical properties.

At supercritical chamber pressures, where the LN_2 jet visually resembles a turbulent gas jet, the growth rate closely follows both the theoretical equation proposed by Dimotakis (1986) and the independently-derived equation by Papamoschou and Roshko (1988). The spreading angle of the jet shear layer also agrees with Brown and Roshko's (1974) spreading angle measurements of an incompressible turbulent mixing layer between helium and nitrogen gases at atmospheric pressure.

These growth rate measurements complement and extend the visualization results of the previous section. At supercritical pressures, not only do the jets have the visual appearance of a turbulent gas jet, but also the growth rates are consistent with incompressible variable-density turbulent jets. At subcritical pressures, cryogenic jets have the same appearance and growth rate as sprays. The transition between the two regimes occurs near the critical pressure. The above conclusions have been demonstrated for the case of a fully-developed turbulence at the jet exit. Other initial conditions have not yet been examined.

Fractal Analysis

The fractal dimension of jets at various pressures ranging from subcritical to supercritical was calculated and compared to results from other researchers. Reference results taken from Sreenivasan and Meneveau (1986) measured the fractal dimensions of a variety of turbulent gas jets, mixing layers and boundary layers. These results indicate a fractal dimension between *1.33* and *1.38*. In addition, the fractal dimension of a turbulent water jet (Dimotakis *et al.* 1983) and of second wind-induced atomization (Taylor and Hoyt 1983) was computed from scanned images.

The fractal dimensions from the above reference cases are shown as horizontal lines in Figure 3. Overlaid on top of these lines are discrete points indicating the fractal dimension of LN_2 jets injected into GN_2 at various chamber pressures. Different methods of calculating the fractal dimension resulted in different values. Several of these are plotted to provide an indication of the uncertainty. At

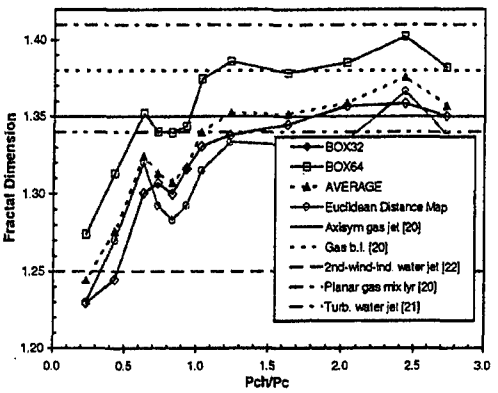

Figure 3. Fractal dimensions of the boundaries of various jets. Discrete points are data from the present effort.

supercritical chamber pressures, the fractal dimension approaches that of turbulent jets and mixing layers. As the chamber pressure is decreased, the fractal dimension also decreases. Below P_r=0.8, the fractal dimension rapidly reduces to a value approximately equal to that of a spray in second wind-induced atomization.

A more thorough discussion of the above results is found in Chehroudi *et al.* (1999). The key observation to be taken is that the results from the fractal analysis complement and extend the previous results. At supercritical pressures, jets have a fractal dimension similar to turbulent gas jets and at subcritical pressures, cryogenic jets have a fractal dimension similar to sprays. The transition occurs at about the same pressure as the transition in visual appearance and growth rate.

Modeling the Growth Rate

Using the data collected on the growth of the cryogenic jet, a semi-empirical equation for the growth rate has been developed. Complete details about the development of this equation are given in Chehroudi *et al.* (1999). The physical reasoning motivating the equation is outlined below.

Previous expressions for the growth rate of sprays and of turbulent jets have a remarkably similar form. Reitz and Bracco (1979) proposed that the growth rate of an isothermal liquid spray could be expressed as

$$\theta \approx 0.27[0 + (\rho_g / \rho_l)^{0.5}].$$

Similarly, Papamoschou and Roshko (1988) suggested the following form for incompressible, but variable density, turbulent jets:

$$\theta = 0.212[1 + (\rho_g / \rho_l)^{0.5}].$$

The similarity in the form of these equations suggests the potential for a link between the two.

It is hypothesized that the transition between the liquid-like and gas-like regimes is governed by the relationship between the time scale necessary for a turbulent structure to be ejected from the jet, τ_b, and the time scale necessary for the structure to dissolve ("vaporize," when subcritical) into the ambient, τ_g. In the liquid-like regime, droplets are ejected from the jet faster then they can vaporize. In the gas-like regime, droplets dissolve faster then they can be thrown off. The transition between the two regimes would be governed by finding the point at which the two times are approximately equal. This is suggested by the comb-like structures seen in Fig 1(b).

Using the above physical models, an equation was proposed for the N_2/N_2 system as

$$\theta = 0.27[(\tau_b /(\tau_b + \tau_g) + (\rho_g / \rho_l)^{0.5}].$$

In the limit, when $\tau_g >> \tau_b$ and $\tau_g \rightarrow \infty$, this equation collapses to the isothermal liquid spray case. This equation agrees well with the current data at subcritical pressures for $\tau_b /(\tau_b + \tau_g) < 0.5$. A constant value of 0.5 was used to predict the spreading rate for higher pressures, including supercritical pressures.

For injection of N_2 into N_2, the characteristic time ratio, $\tau_b /(\tau_b + \tau_g)$, was calculated from experimental measurements of bulge and droplet sizes and calculations of the relevant properties.

For N_2 injection into other gases, however, reliable information about the mixture properties at the interface, particularly the surface tension, prevents such a calculation from being performed. To model these cases, it is hypothesized that the characteristic time ratio is a dominant function of the density ratio, i.e. $\tau_b /(\tau_b + \tau_g) = F(\rho_g / \rho_l)$. Brown and Roshko (1974), indicate that this hypothesis is reasonable because at low Mach numbers there is no distinction between mixing layers where the two streams have different molecular weights, temperatures, or compressibility effects. Measurements of F for the N_2/N_2 system were provided as a plot in Chehroudi *et al.* (1999). A curve fit of that plot gives

$$F(\rho_g / \rho_l) = 5.325\,(\rho_g / \rho_l) + 0.0288 \qquad \rho_g / \rho_l < 0.0885$$

$$= 0.5 \qquad \rho_g / \rho_l \geq 0.0885$$

It was found that the same function, F, calculated from measurements of the N_2/N_2 system could be made to work for other cases, provided that a case-dependant transformation was made to the density ratio at which F is evaluated. The final form of the equation thus arrived at is

$$\theta = 0.27[F(x(\rho_g / \rho_l)) + (\rho_g / \rho_l)^{0.5}]$$

where

x=1.0 for N_2-into-N_2
x=0.2 for N_2-into-He
x=1.2 for N_2-into-Ar

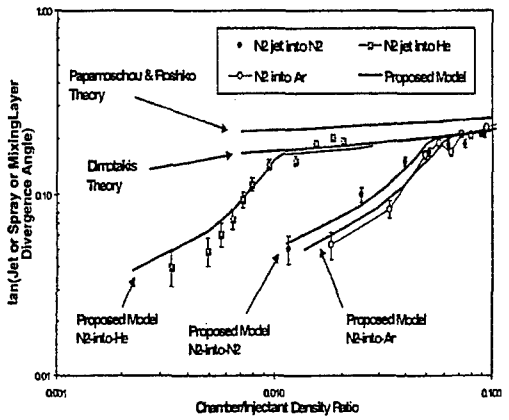

The quality of the agreement with experimental data is demonstrated in Figure 4.

Raman Scattering Measurements

In addition to the line-of-sight shadowgraph images from which the preceeding results have been acquired, spontanenous Raman scattering has also been used to obtain spatially-resolved measurements of the density distrubution within the cryogenic jet. Raman scattered light results from an inelastic collision between light photons and molecules. Since the process is inelastic, the incident beam will be shifted a fixed amount dependent upon the structure of the molecule. Generally, the intensity of the Raman scattered signal yields information on the number density of the gas being examined. A more detailed description of these experiments can be found in Chehroudi *et al.*, 2000.

A thin light sheet was generated using a frequency doubled Nd:YAG laser. Before the beam entered the test section, it passed through an optical delay loop which increased pulse duration from *10 ns* to *36 ns*. Lengthening the pulse was required to reduce the peak laser power, which reduces the possibility of producing stimulated Raman scattering or broadband breakdown caused by the lensing effect of the jet itself. For the *532 nm* incident beam, the Raman-shifted scattered light of N_2 was detected at *607 nm* by an intensified CCD camera equipped with a bandpass filter to reject light at frequencies other then that of the Raman-shifted N_2.

Figure 5 shows typical averaged raw images of the LN_2 jet at sub- and supercritical conditions. The Raman intensity profile for the subcritical case is larger in magnitude at the center of the jet and is narrower in shape then the corresponding image of the supercritical jet.

The full width of the radial profiles measured where the intensity increment was half the maximum (Full-Width-Half-Maximum, FWHM) was extracted from the measured Raman data, and the spreading rate thus measured was compared with the spreading rate measured from the shadowgraph visualizations. The results are plotted in Figure 6. It was found that

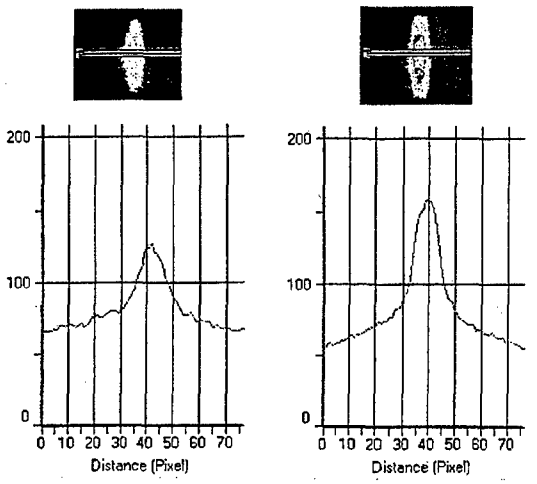

Figure 5. Averaged Raman images of LN_2 jet at sub- and super-critical chamber conditions.

the spreading rate measured at twice the FWHM values of the Raman data agreed well with the shadowgraph measurements. Thus the correspondence of the two different techniques of measuring the width of the jet was established.

Summary and Conclusions

The structure and growth rate of cryogenic jets injected into an ambient with a pressure which ranged from subcritical to supercritical have been studied at AFRL. At subcritical pressures, comparison of shadowgraph measurements show that the jets have the appearance of a conventional liquid spray. As pressure is increased beyond the fluid critical pressure, the structure of the jet changes. Under these conditions, the cryogenic jets have the appearance of turbulent gaseous jets.

A physically based empirical equation was developed based on a mechanism governed by characteristic gasification times and interfacial turbulent bulge formation times to predict growth rate behavior. Spontaneous Raman scattering measurements of the density have been used to confirm the earlier shadowgraph measurements.

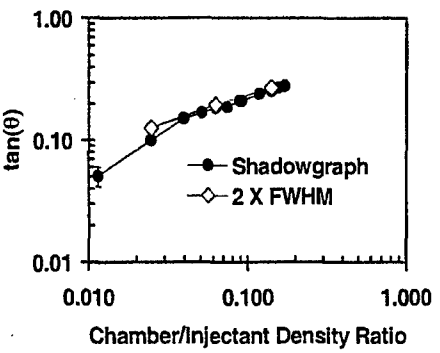

Figure 6. Comparison of the spreading angle of an N_2/N_2 system measured using shadowgraph and spontaneous Raman techniques.

Growth rate measurements derived from the Raman measurements at twice the FWHM distance correspond very closely to the growth rate derived from the shadowgraph measurements.

Research into these phenomena is continuing at AFRL, and we are currently examining the effect of acoustical forcing on sub- and super-critical, cryogenic jets.

Acknowledgements

Mr. Mike Griggs and Mr. Earl Thomas are thanked for their valuable support. Mr. Paul Loftsgard is thanked for his assistance in part of the data acquisition/processing and fractal analysis work. This work is sponsored by the Air Force Office of Scientific Research under Dr. Mitat Birkan, program manager.

References

Anderson, T.J. *et al.,* "Oxygen Concentration Measurements in a High Pressure Environment Using Raman Imaging," AIAA Paper 95-0140.

Brown, G. and Roshko, A. "On density effects and large structure in turbulent mixing layers," *J. Fluid Mech.*, vol. 64, 1974, part 4, pp. 775-816.

Bruno, T. J. and Ely, J. F. *Supercritical fluid technology*, CRC Press, 1991.

Chehroudi, B. *et al.,* "Raman Scattering Measurements in the Initial Region of Sub- and Supercritical Jets," AIAA Paper 2000-3392.

Chehroudi, B. *et al.*, "Fractal geometry and growth rate of cryogenic jets near critical point," AIAA Paper 99-2489.

Chehroudi, B. *et al.*, "Initial Growth Rate and Visual Characteristics of a Round Jet into a Sub- to Supercritical Environment of Relavance to Rocket, Gas Turbine, and Diesel Engines," AIAA paper 99-0206.

Decker, M.C., *et al.* "Quantitative Raman Imaging Investigations of Mixing Phenomena in High Pressure Cryogenic Jets," *Appl Opt* 37:5620-5627, 1998.

Dimotakis, P.E. "Two-dimensional shear-layer entrainment," *AIAA Journal*, 21, No. 11, 1986, pp. 1791-1796.

Dimotakis, P.E. *et al.*, Phy. Fluids, 26, 1983, p. 3185.

Mayer, W. *et al.* "Injection and mixing processes in high pressure LOX/GH2 rocket combustors," AIAA Paper no. 96-2620.

Mayer, W. *et al.* "Propellant atomization in LOX/GH2 rocket combustors," AIAA Paper no. 98-3685.

Naber, J.D. and Siebers, D.L. "Effects of gas density and vaporization on penetration and dispersion of diesel sprays," SAE Paper no. 960034, 1996.

Newman, J.A. and Brzustowski. "Behavior of a liquid jet near the thermodynamic critical region," *AIAA Journal*, vol. 9, 1971, no. 8, pp. 1595-1602.

Oschwald, M. and Schik, A. "Supercritical Nitrogen Free Jet Investigated by Spontaneous Raman Scattering," *Experiments in Fluids*, 27, 497-506, 1999.

Oschwald, M. *et al.* "Investigation of Coaxial LN2/GH2-Injection at Supercritical Pressure by Spontaneous Raman Scattering," AIAA paper no. 99-2887

Papamoschou, D. and Roshko, A. "The compressible turbulent shear layer: an experimental study," *J. Fluid Mech.*, vol. 197, 1988, pp. 453-477.

Reitz, R.D. and Bracco, F.V. "On the dependence of spray angle and other spray parameters on nozzle design and operating condition," SAE Paper no. 790494, 1979.

Sreenivasan, K. R. and Meneveau, C. "The fractal facets of turbulence," *J. Fluid Mech.,* Vol. 173, pp. 357-386, 1986.

Taylor, J.J. and Hoyte J.W., "Water jet photography-Technique and methods," Exp. Fluids, vol. 1, 1983, pp. 113-120.

Woodward, R.D. and Talley, D.G. "Raman imaging of transcritical cryogenic propellants," AIAA Paper 96-0468.